ORIGINAL RESEARCH

Arterial Spin-Labeling and MR Spectroscopy in the Differentiation of Gliomas

S. Chawla
S. Wang
R.L. Wolf
J.H. Woo
J. Wang
D.M. O'Rourke
K.D. Judy
M.S. Grady
E.R. Melhem
H. Poptani

BACKGROUND AND PURPOSE: Noninvasive grading of gliomas remains a challenge despite its important role in the prognosis and management of patients with intracranial neoplasms. In this study, we evaluated the ability of cerebral blood flow (CBF)-guided voxel-by-voxel analysis of multivoxel proton MR spectroscopic imaging (^{1}H-MRSI) to differentiate low-grade from high-grade gliomas.

MATERIALS AND METHODS: A total of 35 patients with primary gliomas (22 high grade and 13 low grade) underwent continuous arterial spin-labeling perfusion-weighted imaging (PWI) and ^{1}H-MRSI. Different regions of the gliomas were categorized as "hypoperfused," "isoperfused," and "hyperperfused" on the basis of the average CBF obtained from contralateral healthy white matter. ^{1}H-MRSI indices were computed from these regions and compared between low- and high-grade gliomas. Using a similar approach, we applied a subgroup analysis to differentiate low- from high-grade oligodendrogliomas because they show different physiologic and genetic characteristics.

RESULTS: $Cho_{glioma\ (G)/white\ matter\ (WM)}$, $Glx_{G/WM}$, and $Lip+Lac_G/Cr_{WM}$ were significantly higher in the "hyperperfused" regions of high-grade gliomas compared with low-grade gliomas. $Cho_{G/WM}$ and $Lip+Lac_G/Cr_{WM}$ were also significantly higher in the "hyperperfused" regions of high-grade oligodendrogliomas. However, metabolite ratios from the "hypoperfused" or "isoperfused" regions did not exhibit any significant differences between high-grade and low-grade gliomas.

CONCLUSION: The results suggest that ^{1}H-MRSI indices from the "hyperperfused" regions of gliomas, on the basis of PWI, may be helpful in distinguishing high-grade from low-grade gliomas including oligodendrogliomas.

The clinical management of glioma presents a considerable challenge, and presurgical grading is important for prognosis and the planning of treatment strategies.[1,2] It has been shown that proton MR spectroscopy (^{1}H-MR spectroscopy) and perfusion-weighted imaging (PWI) can evaluate the degree of malignancy of brain tumors.[3-5] Anecdotal studies[6,7] also report the potential of these techniques in differentiating the grade of oligodendrogliomas, a subgroup of gliomas that possesses unique genetic and physiologic characteristics.[8] Despite favorable results, the ability to use ^{1}H-MR spectroscopy and PWI data in predicting the histologic grade is a subject of considerable controversy, particularly in the subgroup of oligodendrogliomas.[9-13] Owing to inherent heterogeneity of gliomas, ^{1}H-MR spectroscopy indices and perfusion measurements vary considerably, and there are reports of overlap of choline/creatine (Cho/Cr) ratio, relative cerebral blood volume (rCBV), and cerebral blood flow (CBF) values between different grades of glioma.[7,14-17]

There have been some efforts to combine ^{1}H-MR spectroscopy and PWI in characterizing gliomas to improve the accuracy in predicting the tumor grade.[5,15,18] In one study,[19] maximum rCBV was shown to be superior to ^{1}H-MR spectroscopy in predicting glioma grade. On the other hand, Fayed et al[15] reported that ^{1}H-MR spectroscopy was better than rCBV, whereas Yang et al[5] suggested a complementary role of these 2 techniques in separating different grades of the gliomas. One possible explanation for conflicting results in these studies might be that ^{1}H-MR spectroscopy voxels may not have corresponded to regions of maximum CBF or rCBV on PWI. With these limitations in mind, our study was designed to evaluate the hypothesis that the combined voxel-by-voxel analysis of PWI and ^{1}H-MRSI indices can improve the preoperative diagnostic efficacy of these methods in differentiating high-grade from low-grade gliomas including oligodendrogliomas.

Received September 13, 2006; accepted after revision March 27, 2007.

From the Departments of Radiology (S.C., S.W., R.L.W., J.H.W., J.W., E.R.M., H.P.) and Neurosurgery (D.M.O., K.D.J., M.S.G.), University of Pennsylvania, Philadelphia, Penn.

Please address correspondence to Harish Poptani, PhD, University of Pennsylvania, B6 Blockley Hall, 423 Guardian Dr, Philadelphia, PA 19104; e-mail: poptanih@uphs.upenn.edu

DOI 10.3174/ajnr.A0673

Materials and Methods

Subjects

We obtained approval for this study from the Institutional Review Board and informed consent from all patients. For comparison, we retrospectively evaluated 35 subjects (21 men and 14 women; mean age, 45.46 years; age range, 20–68 years) who had histopathologic results. All patients underwent MR examination before surgery, radiation, or chemotherapy. Patients were divided into 2 groups: high-grade (grades 3 and 4, $n = 22$) and low-grade gliomas (grades 1 and 2, $n = 13$). Among those with low-grade gliomas, 11 patients had oligodendrogliomas, 1 patient had an astrocytoma, and 1 had a ganglioglioma. Of the 35 patients, 16 with oligodendrogliomas were included in a separate subgroup analysis. These patients were divided into 2 groups: high-grade (grade 3, $n = 5$) and low-grade (grade 2, $n = 11$). Of these patients, 4 had mixed oligoastrocytomas (3 low-grade and 1 high-grade) with prominent composition of oligodendroglial cells and were thus included in this group (Table 1).

Data Acquisition

Conventional MR Imaging. We performed MR imaging and ^{1}H-MRSI on a 3T Magnetom Trio scanner (Siemens, Erlangen, Germany) equipped with a standard quadrature head coil provided by the manufacturer. The imaging protocol included a 3-plane scout localizer axial 3D T1-weighted magnetization-prepared rapid acquisition

Table 1: Subject demographics

WHO Grade	Histopathologic Grade of the Glioma (1–4)	Number of Subjects
Low grade (n = 13)	Ganglioglioma (1)	1
	Astrocytoma (2)	1
	Oligodendroglioma (2)	11
High grade (n = 22)	Astrocytoma (3)	4
	Oligodendroglioma (3)	5
	Glioblastoma multiforme (4)	13

Note:—WHO indicates World Health Organization.

of gradient echo (MPRAGE) (TR 1620 ms; TE, 3.9 ms; TI, 950 ms, 192 × 256 matrix size, 1-mm section thickness); and axial fluid-attenuated inversion recovery (FLAIR) (TI, 2500 ms; TR, 9190 ms; TE, 97 ms) or axial T2-weighted turbo spin-echo (TR, 4000 ms; TE, 85 ms) sequences.

PWI. For continuous arterial spin-labeling (CASL) perfusion MR imaging, twelve 6-mm-thick axial sections with a 1.5-mm intersection gap were acquired. Other parameters included FOV, 22 × 22 cm^2; matrix size, 64 × 64 (3.44 mm in-plane resolution); TR, 4000 ms; and TE, 17 ms. We applied the labeling for the control pulse at the level of the cervicomedullary junction by using a postlabeling delay of 1.2 s and labeling duration of 2 s,[20] along with radio frequency (RF) amplitude of 2.25T and a gradient strength of 1.6 mT/m for the labeling pulses. These power levels were within the FDA guidelines for RF deposition and provided a labeling efficiency of 68%.[21] We implemented the control pulses by using amplitude modulation of labeling pulses on the basis of a sinusoid function with a frequency of 100 Hz.

^{1}H-MRSI. We performed a 2D multivoxel ^{1}H-MRSI by using a spin-echo (point-resolved spectroscopy) sequence with water suppression by means of selective excitation. Sequence parameters included TR, 1700 ms; TE, 30 ms; NEX, 3; FOV, 16 × 16 cm^2; section thickness, 15 to 20 mm; bandwidth, 1200 Hz; and matrix size, 16 × 16 to obtain a good signal-to-noise ratio within a reasonable acquisition time of 7 minutes. We selected the volume of interest (VOI) to include the neoplasm as well as areas of normal-appearing contralateral brain parenchyma, avoiding the scalp, base of the skull, or sinuses. We placed 8 outer volume saturation slabs (30-mm thick) outside the VOI to suppress lipid signals from the scalp. We acquired the dataset by using elliptical *k*-space sampling with weighted phase encoding to reduce the acquisition time. To minimize the effect of increased nominal voxel size by elliptical *k*-space sampling, we applied a Hanning filter (50%) in the spatial dimensions. We then performed manual shimming to achieve an optimum full width at half maximum value (FWHM <20 Hz) of the water signal intensity.

Data Analysis

PWI. We processed perfusion data off-line by using a program written in interactive data language (IDL) software (Research Systems, Boulder, Colo). The PWI series was generated by pair-wise subtraction of the label and control images followed by conversion to absolute CBF map on the basis of a 2-compartment CASL perfusion model.[21] The resulting CBF maps were coregistered with T1-weighted MPRAGE images with use of statistical parametric mapping software (SPM99; Wellcome Trust Centre for Neuroimaging, London, UK). We performed the analysis of the PWI maps in 3 ways:

Because maximum perfused regions of the gliomas are suggestive of malignancy and aggressiveness,[22] we analyzed the PWI data from the 3 maximally perfused regions of the entire volume of the glioma by drawing regions of interest (ROIs) comprising 30 pixels as the first analytical method. We averaged the values from these regions and normalized them to the contralateral normal white matter (NWM). These values are reported as $CBF_{maximum\ (max)}$ and $CBF_{max/\ white\ matter\ (WM)}$, respectively.

In the second method, we measured CBF by drawing ROIs in the glioma from the 3 sections that corresponded to the approximate section thickness and location of the ^{1}H-MRSI VOI. The ROIs were initially generated on coregistered T1-weighted MPRAGE images because these images are acquired at higher spatial resolution, providing a more accurate delineation of the tissue. The CBF values from these ROIs were then noted from the coregistered CBF maps. As with the first method, we averaged the data and normalized them to the contralateral NWM. These values are represented as CBF_{total} or $CBF_{total/WM}$, respectively.

In the third method of data analysis, we separated the glioma into 3 different categories as "hypoperfused," "isoperfused," and "hyperperfused" with respect to the contralateral NWM to assess the heterogeneity of CBF in the neoplasm. Different regions of the gliomas were categorized as "hyperperfused" if average CBF was more than 1 SD (25.86 mL/100 g/min), "hypoperfused" if less than 1 SD (20.45 mL/100 g/min), or "isoperfused" if CBF was within 1 SD of the mean value of CBF in NWM (20.45–25.86 mL/100 g/min). Average CBF from these areas were then normalized to the contralateral NWM and reported as $CBF_{glioma\ (G)/WM}$.

^{1}H-MRSI. We analyzed the ^{1}H-MRSI data from voxels (n = 4–13) that encompassed the glioma and exhibited good spectral resolution (FWHM <20Hz) and signal-to-noise ratio. The region between 0.2 and 4.0 ppm of the spectrum was processed. We evaluated the following ^{1}H-MRSI indices: *N*-acetylaspartate (NAA), 2.02 ppm; Cr, 3.02 ppm; Cho, 3.22 ppm; myo-inositol (mIns), 3.56 ppm; and glutamine/glutamate (Glx), 2.35 ppm. The resonance at 1.3 ppm was assigned to a combination of lactate (Lac) and lipid (Lip) since it is difficult to differentiate contributions from Lac and Lip. We measured the absolute concentrations of metabolites by using a user-independent spectral fit program (linear combinations of models).[23] To compare the ^{1}H-MR spectroscopy findings with the PWI data, we analyzed the ^{1}H-MRSI data according to the second and third approaches of the PWI data analysis:

In the first method, concentrations of each metabolite from the voxels (n = 4–13) covering the glioma were averaged and normalized to the voxels (n = 3–10) of the contralateral NWM. To avoid the effects resulting from variations in the intertumor and intratumor energy metabolism, we did not use concentration of Cr as a reference from the same voxel.

In the second method, a spectroscopic grid overlaid over a T1-weighted image was used to match the voxels of ^{1}H-MRSI with different regions of gliomas on CBF map. Concentrations of metabolites of the voxels from "hyperperfused" (n = 3–12), "hypoperfused" (n = 1–5), and "isoperfused" (n = 1–6) regions of the glioma were individually normalized to the voxels in the contralateral NWM and averaged. Because Lip and Lac peaks are not observed in the normal brain, Lip+Lac from the voxels encompassing the glioma were normalized with respect to Cr from the NWM.

We also performed a similar subgroup analysis between low-grade (grade 2, n = 11) and high-grade oligodendrogliomas (grade 3, n = 5).

Statistical Analysis

We used a 2-tailed heteroscedastic Student *t* test to look for differences in CBF_{total}, $CBF_{total/WM}$, CBF_{max}, and $CBF_{max/WM}$ between low-grade and high-grade gliomas. A comparison between $CBF_{total/WM}$ and ^{1}H-MRSI

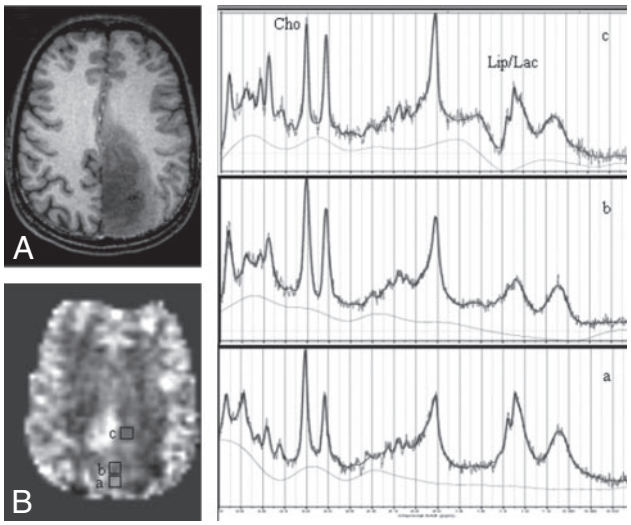

Fig 1. Axial T1-weighted MPRAGE image (*A*) demonstrates a low-grade oligodendroglioma in the left parietal region; CBF map (*B*) shows voxels from "hyperperfused" (*a*), "isoperfused" (*b*), and "hypoperfused" (*c*) regions. ^{1}H-MRSI spectra (*a-c*) are from the corresponding voxels shown on the CBF map.

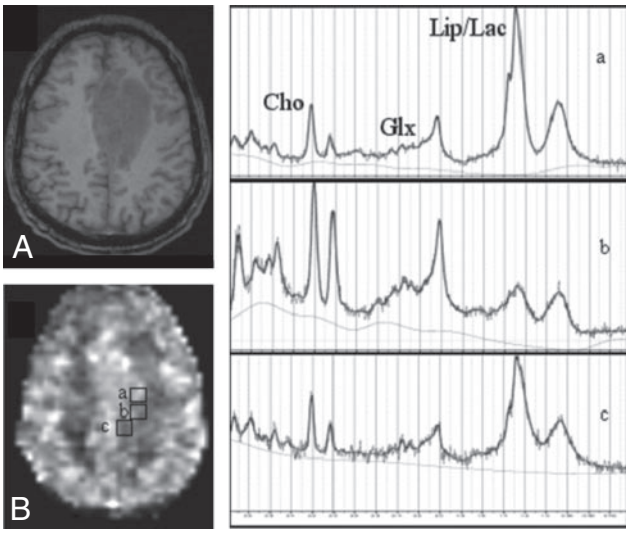

Fig 2. Axial T1-weighted MPRAGE image (*A*) exhibits a case of GBM in the frontal lobe; CBF map (*B*) shows voxels from "hyperperfused" (*a*), "isoperfused" (*b*), and "hypoperfused" (*c*) regions of the glioma. ^{1}H-MRSI spectra (*a–c*) are from the corresponding voxels shown on the CBF map.

indices from the central 3 sections corresponding to the ^{1}H- MRSI VOI was performed. We also performed an independent comparison of $CBF_{G/WM}$ and ^{1}H-MRSI indices from the "hypoperfused," "isoperfused," and "hyperperfused" regions of the glioma to differentiate low-grade from high-grade gliomas. A similar statistical approach was also applied for the subgroup analysis of oligodendrogliomas. A probability (P) value of $<.05$ was considered significant. Confidence intervals (CI, 95%) of $Cho_{G/WM}$, $Glx_{G/WM}$, and $Lip+Lac_G/Cr_{WM}$ from low-grade and high-grade gliomas and $Cho_{G/WM}$ and $Lip+Lac_G/Cr_{WM}$ from oligodendrogliomas were also computed.

Results

In general, high-grade gliomas showed foci of increased CBF, higher Cho, Lac+Lip, and Glx than low-grade gliomas (Figs 1, 2). We found significantly different CBF_{max} between low-grade (51.34 ± 16.85 mL/100 g/min) and high-grade (88.48 ± 65.28) gliomas ($P < .05$). However, CBF_{total} from the 3 central sections from the glioma corresponding to the ^{1}H-MRSI section was not significantly different between low-grade (37.28 ± 12.68) and high-grade (41.50 ± 18.48) gliomas ($P > .05$). Even when CBF was normalized to the contralateral NWM ($CBF_{total/WM}$), the difference between low-grade (1.68 ± 0.44) and high-grade (1.90 ± 0.75) gliomas was not significant ($P > .05$).

When we compared ^{1}H-MRSI data from all the voxels in the glioma with CBF_{total} from the 3 central sections between low-grade and high-grade gliomas, we observed higher $Cho_{total/WM}$ (1.58 ± 0.41 vs 1.35 ± 0.32), $Glx_{total/WM}$ (1.24 ± 0.51 vs 1.18 ± 0.37), and $Lip+Lac_{total}/Cr_{WM}$ (4.03 ± 3.24 vs 2.54 ± 0.73) in the high-grade gliomas compared with low-grade. However, no significant difference was obtained for any of the ^{1}H-MRSI indices ($P > .05$).

The percentage of voxels with "hypoperfused," "isoperfused," and "hyperperfused" CBF values from the central 3 sections of low-grade gliomas was 31.05%, 30.56%, and 38.35%, respectively, whereas 17.13%, 27.67%, and 55.33% voxels had CBF values corresponding to the "hypoperfused," "isoperfused," and "hyperperfused" regions in high-grade gliomas. It was not possible to differentiate low-grade from high-grade gliomas on the basis of $CBF_{G/WM}$ alone ($P > .05$). However, on ^{1}H-MRSI, $Cho_{G/WM}$ (2.11 ± 0.46 vs 1.15 ± 0.31), $Glx_{G/WM}$ (1.01 ± 0.52 vs 0.63 ± 0.21) and $Lip+Lac_G/Cr_{WM}$ (6.83 ± 4.17 vs 2.23 ± 0.65) were significantly higher in the "hyperperfused" high-grade gliomas compared with low-grade ($P < .05$). The CI (95%) of $Cho_{G/WM}$ for low-grade and high-grade gliomas was 1.02 to 1.28 and 1.88 to 2.34, respectively. CI (95%) of $Glx_{G/WM}$ for low-grade and high-grade gliomas was 0.53 to 0.73 and 0.9 to 1.12, respectively. CI (95%) of $Lip+Lac_G/Cr_{WM}$ for low-grade and high-grade gliomas was 1.67 to 2.79 and 5.13 to 8.53, respectively. There was no significant difference in the other metabolites (NAA, Cr, or mIns) between the 2 grades in the "hyperperfused" areas. Metabolite ratios from the "hypoperfused" or "isoperfused" regions did not exhibit any significant differences between the 2 glioma groups (Table 2). The $Cho_{G/WM}$, $Glx_{G/WM}$, and $Lip+Lac_G/Cr_{WM}$ values from low-grade and high-grade gliomas are shown as scatterplots in Fig 3.

In the subgroup of patients with oligodendrogliomas, all 4 perfusion indices (CBF_{total}, $CBF_{total/WM}$, CBF_{max}, and $CBF_{max/WM}$) were not significantly different between the low-grade (grade 2) and high-grade (grade 3) oligodendrogliomas ($P > .05$). Moreover, $CBF_{G/WM}$ from the "hyperperfused," "isoperfused," or "hypoperfused" regions could not differentiate the 2 grades of oligodendrogliomas ($P > .05$). However, on ^{1}H-MRSI, $Cho_{G/WM}$ (2.20 ± 0.35 vs 1.16 ± 0.25) and $Lip+Lac_G/Cr_{WM}$ (5.15 ± 0.68 vs 2.64 ± 0.65) were significantly higher in the "hyperperfused" regions of high-grade oligodendrogliomas compared with low-grade ($P < .05$). CI (95%) of $Cho_{G/WM}$ for low-grade and high-grade oligodendrogliomas was 1.01 to 1.31 and 2.02 to 2.58, respectively. CI (95%) of $Lip+Lac_G/Cr_{WM}$ for low-grade and high-grade oligodendrogliomas was 2.24 to 3.04 and 4.61 to 5.69, respectively. There was no significant difference in the other metabolites (NAA, Cr, mIns, or Glx) between the 2 grades in the "hyperperfused" areas. None of

Table 2: CBF and metabolite ratios from different regions of gliomas

Glioma Region	$CBF_{G/WM}$	$NAA_{G/WM}$	$Cr_{G/WM}$	$Cho_{G/WM}$	$mIns_{WM}$	$Glx_{G/WM}$	$Lip+Lac_G/Cr_{WM}$
	Low Grade						
Hyperperfused	1.73 ± 0.62	0.51 ± 0.11	0.74 ± 0.17	1.15 ± 0.31	1.16 ± 0.31	0.63 ± 0.21	2.23 ± 0.65
Hypoperfused	0.79 ± 0.09	0.62 ± 0.27	0.96 ± 0.34	1.41 ± 0.57	1.20 ± 0.52	0.60 ± 0.12	2.20 ± 0.63
Isoperfused	0.93 ± 0.09	0.56 ± 0.12	0.89 ± 0.26	1.49 ± 0.15	1.18 ± 0.38	0.68 ± 0.24	1.44 ± 0.59
	High Grade						
Hyperperfused	1.94 ± 0.47	0.46 ± 0.17	0.73 ± 0.27	2.11 ± 0.46*	1.39 ± 0.55	1.01 ± 0.52*	6.83 ± 4.17*
Hypoperfused	0.87 ± 0.07	0.46 ± 0.07	0.70 ± 0.20	1.55 ± 0.4	1.18 ± 0.43	0.78 ± 0.14	2.87 ± 1.13
Isoperfused	0.98 ± 0.1	0.40 ± 20	0.71 ± 0.19	1.71 ± 0.59	1.42 ± 0.73	0.71 ± 0.12	2.21 ± 1.05

Note:—CBF indicates cerebral blood flow; $_{G/WM}$, glioma/white matter; Cr, creatine; Cho, choline; mIns, myo-inositol; Glx, glutamine/glutamate; Lip+Lac, lipid and lactate.
* Significantly higher ($P < .05$) compared with low-grade glioma.

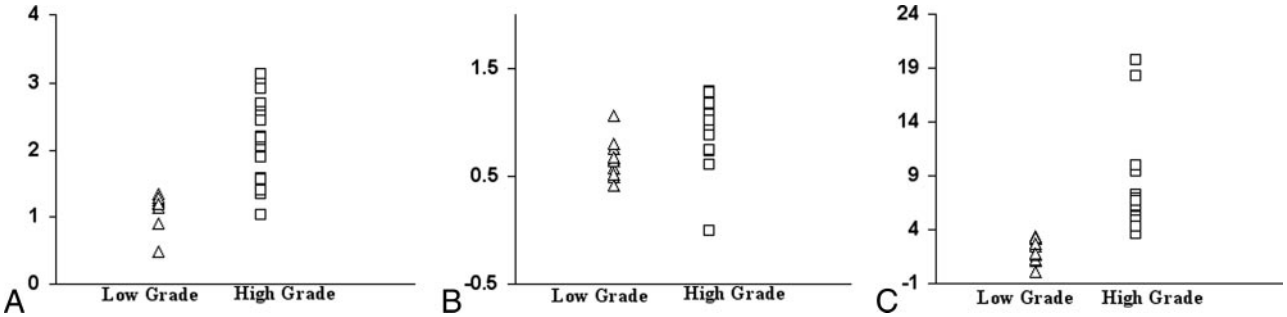

Fig 3. Scatterplots demonstrate the variations in $Cho_{G/WM}$ (*A*), $Glx_{G/WM}$, (*B*), and $Lip+Lac_G/Cr_{WM}$ (*C*) from the "hyperperfused" regions between the low-grade and high-grade gliomas.

Table 3: CBF and ^{1}H-MRSI indices from different regions of oligodendrogliomas

Oligodendroglioma Region	$CBF_{Oligo/WM}$	$NAA_{Oligo/WM}$	$Cr_{Oligo/WM}$	$Cho_{Oligo/WM}$	$mIns_{Oligo/WM}$	$Glx_{Oligo/WM}$	$Lip+Lac_{Oligo}/Cr_{WM}$
	Grade 2						
Hyperperfused	1.70 ± 0.53	0.49 ± 0.13	0.73 ± 0.16	1.16 ± 0.25	1.17 ± 0.24	0.65 ± 0.24	2.64 ± 0.65
Hypoperfused	0.73 ± 0.12	0.46 ± 0.10	0.80 ± 0.26	1.39 ± 0.28	1.07 ± 0.27	0.59 ± 0.12	2.73 ± 0.79
Isoperfused	0.93 ± 0.17	0.48 ± 0.15	0.85 ± 0.14	1.49 ± 0.4	1.18 ± 0.42	0.68 ± 0.24	1.82 ± 0.3
	Grade 3						
Hyperperfused	2.16 ± 0.37	0.44 ± 0.14	0.71 ± 0.13	2.20 ± 0.35*	1.30 ± 0.16	0.89 ± 0.30	5.15 ± 0.68*
Hypoperfused	0.78 ± 0.14	0.44 ± 0.15	0.69 ± 0.22	1.69 ± 0.36	1.36 ± 0.33	0.61 ± 0.24	3.22 ± 0.1.12
Isoperfused	0.97 ± 0.19	0.42 ± 0.12	0.69 ± 0.22	1.64 ± 0.69	1.34 ± 0.88	0.72 ± 0.12	2.56 ± 0.85

Note:—CBF indicates cerebral blood flow; NAA, *N*-acetylaspartate; $_{Oligo/WM}$, oligodendroglioma/white matter; Cr, creatine; Cho, choline; mIns, myo-inositol; Glx, glutamine/glutamate; Lip+Lac, lipid and lactate.
* Significantly higher ($P < .05$) compared with grade 2 oligodendrogliomas.

the metabolite ratios from the "hypoperfused" or "isoperfused" regions exhibited any significant differences between the 2 oligodendroglioma groups (Table 3). The scatterplots of $ChoG_{/WM}$ and $Lip+Lac_G/Cr_{WM}$ between the low-grade and high-grade oligodendrogliomas demonstrate this variability in the 2 groups (Fig 4).

Discussion

From a histologic standpoint, gliomas are heterogeneous, with components that include varying degrees of cellular and nuclear pleomorphism, mitotic activity, vascular proliferation, and necrosis.[24,25] Our results show that if the analysis of ^{1}H-MRSI data are restricted to the "hyperperfused" regions, it is possible to differentiate high-grade gliomas from low-grade ones.

In the present study, we used CBF-guided voxel-by-voxel analysis of ^{1}H-MRSI to evaluate the efficacy of this method in differentiating low-grade from high-grade gliomas. Although arterial spin-labeling (ASL) techniques may not be available in all clinical scanners, we believe that MRSI analysis guided by blood volume data may equally be used with methods that use the dynamic susceptibility contrast (DSC) enhancement to measure relative cerebral blood volume (rCBV). A close correlation between DSC and ASL techniques for determination of blood flow in brain tumors has recently been reported.[26] Postcontrast-enhanced T1-weighted images can also be potentially used to select the MRSI voxels of interest. However, contrast enhancement is not always accurate in predicting the grade of a tumor, and all high-grade tumors do not enhance.[27] Moreover, it has been shown previously that metabolic abnormality extends beyond the contrast-enhanced areas in brain tumors.[12] Perfusion-weighted images (ASL, DSC, or dynamic contrast enhanced), reflect true alterations in the physiology of a tumor.[28] Thus, we believe that analysis of PWI-guided ^{1}H-MRSI indices may allow more sensitive differentiation of glioma grades than contrast-enhanced image analysis.

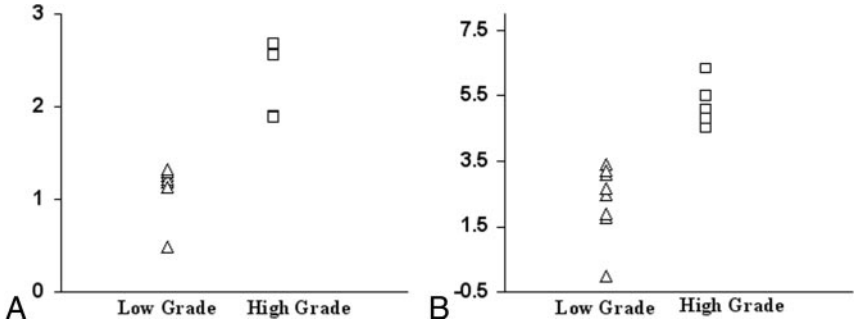

Fig 4. Scatterplots demonstrate the variations in $Cho_{G/WM}$ (*A*), and $Lip+Lac_G/Cr_{WM}$ (*B*) from the "hyperperfused" regions between the low-grade and high-grade oligodendrogliomas.

Significantly elevated CBF_{max} and $CBF_{max/WM}$ were found in high-grade gliomas compared with low-grade ones, and our results are in agreement with reports in the literature.[14,19] However, in a subgroup analysis of oligodendrogliomas, there was no significant difference in CBF_{max} and $CBF_{max/WM}$ between the 2 grades. Oligodendroglial tumors, which consist of oligodendrogliomas and mixed oligoastrocytomas, account for 5% to 18% of all gliomas.[29] Combined loss of heterozygosity (LOH) on chromosomal arms 1p and 19q are molecular signatures that distinguish oligodendrogliomas from other subtypes of gliomas. LOH 1p/19q has emerged as an independent predictive marker of better response to radiotherapy and chemotherapy as well as longer survival in patients with anaplastic oligodendroglial tumors.[30-33] In a recent report, Spampinato et al[6] have successfully separated low-grade from high-grade oligodendrogliomas on the basis of maximum rCBV values. However, few studies have reported high perfusion from low-grade oligodendrogliomas and low perfusion from high-grade oligodendrogliomas.[7,14,22] In a previous study, Wolf et al[14] reported normalized CBF_{max} of less than one in 2 cases of gliomas, which were later found to be grade 3 gliomas with oligodendroglial components. Using a DSC perfusion MR imaging technique, Xu et al[7] did not find any difference between low-grade and high-grade oligodendrogliomas. Similarly, Lev et al[22] reported a poor correlation between tumor perfusion and grade in a subpopulation of 8 oligodendrogliomas. These observations may reflect the inherently vascular nature of some low-grade oligodendrogliomas, which have been classically described as having a attenuated network of branching capillaries.[34] The possible explanation for the successful attempt by Spampinato et al[6] in differentiating the 2 grades of oligodendrogliomas may be that these authors used smaller ROIs than used in previous studies and thus avoided volume averaging.

Although no tumor-specific metabolite is detectable with in vivo ^{1}H-MR spectroscopy, it is possible to detect specific changes in the pattern of spectral features of a tumor that are different from those of the normal brain. Few studies have shown the potential of ^{1}H-MR spectroscopy to differentiate low-grade from high-grade gliomas[3-5,19] including oligodendrogliomas.[6,7] The authors of these studies have observed significantly higher maximum Cho/Cr in high-grade gliomas compared with low-grade ones. Even with these promising results, the objective of accurately grading gliomas on the basis of ^{1}H-MR spectroscopy findings alone has not been completely achieved.[9-13] In general, Cho is higher in high-grade gliomas.[3,4,35] However, some glioblastoma multiformes (GBMs) have been reported to have low Cho levels.[36] On the other hand, there are also reports of elevated Cho in low-grade gliomas compared with high-grade ones.[19] In our study, when ^{1}H-MRSI data from all the voxels in the glioma were compared with CBF from the glioma involving 3 central sections, no significant difference was obtained for any of the ^{1}H-MRSI indices between low-grade and high-grade gliomas, probably because of the averaging effect by heterogeneous voxels encompassing the glioma. However, when we performed a voxel-by-voxel analysis of ^{1}H-MRSI indices, we observed a significantly higher $Cho_{G/WM}$, $Glx_{G/WM}$, and $Lip+Lac_G/Cr_{WM}$ in high-grade compared with low-grade gliomas only from the "hyperperfused" regions. However, oligodendrogliomas still pose a challenge.

Cho compounds (choline, phosphocholine, and glycerophosphocholine) are part of the normal phospholipid pathways that maintain the integrity of the cell membrane and its associated biochemical functions. These compounds are thought to be markers for increased membrane turnover or high cell number.[37-40] Regions of high rCBV have been correlated with increased mitotic activity,[8] indicating high cell proliferation and thus increased Cho, as observed in our study. Most gliomas demonstrate elevated rCBV that has been correlated with neovascularity.[8,22,41] It has been suggested that hypoxia is one of the leading factors for the development of angiogenesis.[42] In tumors, rapid proliferation of cells leads to hypoxic regions that are distal to the nearby vasculature. Under hypoxic conditions, increased anaerobic glycolysis may lead to an elevation of Lac in the tumor. Overexpression of the hypoxia-inducible factor -1 (HIF1α) may stimulate the dilation of existing vessels or generation of new blood vessels, initiating the process of angiogenesis.[43] The resultant heterogeneous perfusion, in addition to elevated metabolic rates, leads to even more hypoxic regions. This cycle of events ultimately leads to energy failure and cell death that results in necrosis. Although gross regions of necrosis can be imaged by MR imaging, areas of micronecrosis that occur before this situation are hard to detect by conventional T2- or T1-weighted MR imaging. The presence of Lip in MR spectra of tumors has, in fact, been attributed to micronecrosis.[5,19,44] We believe that the presence of significantly elevated Lip and Lac in high-grade gliomas in our study is the result of a combined process of hypoxia, microscopic cellular necrosis, and cell proliferation in "hyperperfused" regions of the gliomas.

Anecdotal in vivo ^{1}H-MR spectroscopy studies have reported high Glx (glutamate [Glu] and glutamine [Gln]) in meningiomas and GBM relative to a normal brain.[45] Elevated Glx has also been observed on in vitro ^{1}H-MR spectroscopy studies of perchloric acid extracts of GBM specimens.[46,47] In our study, we observed significantly high $Glx_{G/WM}$ from the "hyperperfused" regions of the high-grade gliomas compared with the low-grade gliomas. In the subgroup analysis of oligodendrogliomas, higher $Glx_{G/WM}$ was also observed in high-grade oligodendrogliomas; however, this difference was not significant. Bouzier et al[48] reported that Glx is necessary for C6

glioma growth in vivo and is taken up from the blood. In addition to its role as an energy fuel, Glx is also involved in the cellular anabolic pathways. In particular, it is essential for the synthesis of purine and pyrimidine bases as a carbon (via aspartate) and nitrogen donor and therefore necessary for tumor cell growth.[49] Some authors have also reported tumors as being a Glx trap.[50] Tumors have been shown to release Glu at high levels, which may stimulate tumor cell proliferation via activation of Glu receptors. Glu has also been found to facilitate tumor invasion by causing excitotoxic damage to normal brain, thereby paving a pathway for tumor migration.[51] We believe that increased mitotic activity of glioma cells in the "hyperperfused" regions may necessitate the need for Glx. High $Glx_{G/WM}$ was also observed in the "isoperfused" and "hypoperfused" regions of the tumors; however, the difference between low-grade and high-grade gliomas was not significant. The precise explanation for this behavior in not known. However, this may be attributed to the reduced mitotic activity resulting from decreased blood flow in these regions. Therefore, it may be necessary to target the "hyperperfused" regions of the gliomas and look for a metabolite pattern on ^{1}H-MRSI to differentiate low-grade from high-grade gliomas.

^{1}H-MR spectroscopy of brain tumors has been performed with use of different TE for the acquisition of spectra.[10,13,52] A long TE (270 ms) allows observation of a reduced number of metabolites; the spectrum has less baseline distortion and is easy to process, analyze, and interpret. At an intermediate TE of 135 ms, the Lac doublet is inverted because of J-coupling, which makes it easier to differentiate it from Lip and other macromolecules. However, at short TE (20–30 ms), many more metabolites (Lip, mIns, and Glx) are observed in addition to NAA, Cr, and Cho. Because of the relatively short T2 values, signals from these compounds may be attenuated or may completely disappear at higher or intermediate TE. These short T2 metabolites play an important role in the diagnosis and characterization of brain tumors.[10,13,53] Majós et al[54] have also advocated the use of short TE ^{1}H-MR spectroscopy to classify tumors into different grades. In our study, we used a short TE (30 ms), and we assigned the resonance at 1.3 ppm as a combination of both Lac and Lip. Care was taken to avoid contamination of Lip signals from the scalp and bone by placing outer volume saturation slabs around the VOI. To reduce the acquisition time, we used a TR of 1700 ms in our study, which may not have been long enough for the complete relaxation of metabolites. We used the linear combinations of models software to quantify metabolite concentrations, which takes into account the effect of sequence parameters and tissue T1 and T2 values at particular field strength. Moreover, because the metabolite concentration from the tumor was normalized to that of the contralateral NWM, any adverse effects in quantification as a result of the intermediate TR might not have contributed to the overall results, as has been reported previously.[55]

We observed a significant difference in the CBF_{max} values from high-grade and low-grade gliomas; however, this difference was not observed when oligodendrogliomas were analyzed separately. Because it may be difficult to predict the tumor subtype presurgically on the basis of radiologic diagnosis alone, we believe that inclusion of voxel-by-voxel analysis of ^{1}H-MRSI will aid in separating low-grade from high-grade gliomas regardless of the histologic subtypes, including oligodendrogliomas.

A limitation of our study was that most of the patients (84.61%) among the low-grade glioma group were comprised of oligodendrogliomas. Although we did not have any selection bias for this group, incidentally most of the patients with low-grade gliomas turned out to be low-grade oligodendrogliomas, which substantially biased our study toward oligodendrogliomas. Another limitation of our study was that we performed 2D ^{1}H-MRSI that limited the correlation with CBF maps from only 3 sections corresponding to the thickness of VOI. To cover the whole, or at least the bulk of the tumor volume, it will be necessary to use a 3D ^{1}H-MRSI sequence with higher spatial resolution. Multisection or 3D chemical shift imaging studies with higher spatial resolution would also help in a better voxel-to-voxel correlation of the ^{1}H-MR spectroscopy with PWI studies. However, multisection or 3D MRSI techniques lead to increased acquisition time that could be prohibitive in routine clinical settings. A strategy to overcome this shortcoming may be the use of parallel MR spectroscopy imaging (sensitivity encoding or generalized auto-calibrated, partially parallel acquisitions) or echo-planar spectroscopic imaging techniques. Our study was also limited by the fact that separation of gliomas into 3 different categories as "hypoperfused," "isoperfused," and "hyperperfused" with respect to the contralateral NWM was based on a simplistic, manually selected, region-of-interest-based method. To accurately match the CBF voxels with the MRSI voxels, we would need a rigorous approach of tissue segmentation.

Conclusion

Our results suggest the complementary role of PWI and ^{1}H-MRSI in the prediction of grading gliomas. We believe that PWI-guided voxel-by-voxel analysis of ^{1}H-MRSI indices from the regions of high blood flow may be helpful in distinguishing low-grade from high-grade gliomas, including oligodendrogliomas.

Acknowledgments

The authors thank MR imaging coordinators Lisa M. Desiderio and Shannon D'Arcy and technologists Norman Butler, Doris Cain, and Tonya Kurtz for their support.

References

1. Kaba SE, Kyritsis AP. **Recognition and management of gliomas.** *Drugs* 1997;53:235–44
2. Davies E, Hopkins A. **Good practice in the management of adults with malignant cerebral glioma: clinical guidelines. Working Group, Royal College of Physicians.** *Br J Neurosurg* 1997;11:318–30
3. Hsu YY, Chang CN, Wie KJ, et al. **Proton magnetic resonance spectroscopic imaging of cerebral gliomas: correlation of metabolite ratios with histopathologic grading.** *Chang Gung Med J* 2004;27:399–407
4. Herminghaus S, Dierks T, Pilatus U, et al. **Determination of histopathological tumor grade in neuroepithelial brain tumors by using spectral pattern analysis of in vivo spectroscopic data.** *J Neurosurg* 2003;98:74–81
5. Yang D, Korogi Y, Sugahara T, et al. **Cerebral gliomas: prospective comparison of multivoxel 2D chemical-shift imaging proton MR spectroscopy, echoplanar perfusion and diffusion-weighted MRI.** *Neuroradiology* 2002;44:656–66
6. Spampinato MV, Smith JK, Kwock L, et al. **Cerebral blood volume measurements and proton MR spectroscopy in grading of oligodendroglial tumors.** *AJR Am J Roentgenol* 2007;188:204–12
7. Xu M, See SJ, Ng WH, et al. **Comparison of magnetic resonance spectroscopy and perfusion-weighted imaging in presurgical grading of oligodendroglial tumors.** *Neurosurgery* 2005;56:919–26

8. Aronen HJ, Gazit IE, Louis DN, et al. **Cerebral blood volume maps of gliomas: comparison with tumor grade and histologic findings.** *Radiology* 1994;191:41–51
9. Sabatier J, Ibarrola D, Malet-Martino M, et al. [**Brain tumors: interest of magnetic resonance spectroscopy for the diagnosis and the prognosis**]. *Rev Neurol (Paris)* 2001;157:858–62
10. Negendank WG, Sauter R, Brown TR, et al. **Proton magnetic resonance spectroscopy in patients with glial tumors: a multicenter study.** *J Neurosurg* 1996;84:449–58
11. Cheng LL, Chang IW, Louis DN, et al. **Correlation of high-resolution magic angle spinning proton magnetic resonance spectroscopy with histopathology of intact human brain tumor specimens.** *Cancer Res* 1998;58:1825–32
12. McKnight TR, von dem Bussche MH, Vigneron DB, et al. **Histopathological validation of a three-dimensional magnetic resonance spectroscopy index as a predictor of tumor presence.** *J Neurosurg* 2002;97:794–802
13. Tate AR, Majos C, Moreno A, et al. **Automated classification of short echo time in in vivo 1H brain tumor spectra: a multicenter study.** *Magn Reson Med* 2003;49:29–36
14. Wolf RL, Wang J, Wang S, et al. **Grading of CNS neoplasms using continuous arterial spin labeled perfusion MR imaging at 3 Tesla.** *J Magn Reson Imaging* 2005;22:475–82
15. Fayed N, Modrego PJ. **The contribution of magnetic resonance spectroscopy and echoplanar perfusion-weighted MRI in the initial assessment of brain tumours.** *J Neurooncol* 2005;72:261–65
16. Magalhaes A, Godfrey W, Shen Y, et al. **Proton magnetic resonance spectroscopy of brain tumors correlated with pathology.** *Acad Radiol* 2005;12:51–57
17. Gupta RK, Cloughesy TF, Sinha U, et al. **Relationships between choline magnetic resonance spectroscopy, apparent diffusion coefficient and quantitative histopathology in human glioma.** *J Neurooncol* 2000;50:215–26
18. Law M, Cha S, Knopp EA, et al. **High-grade gliomas and solitary metastases: differentiation by using perfusion and proton spectroscopic MR imaging.** *Radiology* 2002;222:715–21
19. Law M, Yang S, Wang H, et al. **Glioma grading: sensitivity, specificity, and predictive values of perfusion MR imaging and proton MR spectroscopic imaging compared with conventional MR imaging.** *AJNR Am J Neuroradiol* 2003;24:1989–98
20. Alsop DC, Detre JA. **Reduced transit-time sensitivity in noninvasive magnetic resonance imaging of human cerebral blood flow.** *J Cereb Blood Flow Metab* 1996;16:1236–49
21. Wang J, Zhang Y, Wolf RL, et al. **Amplitude-modulated continuous arterial spin-labeling 3.0-T perfusion MR imaging with a single coil: feasibility study.** *Radiology* 2005;235:218–28
22. Lev MH, Ozsunar Y, Henson JW, et al. **Glial tumor grading and outcome prediction using dynamic spin-echo MR susceptibility mapping compared with conventional contrast-enhanced MR: confounding effect of elevated rCBV of oligodendrogliomas** [published erratum appears in *AJNR Am J Neuroradiol* 2004;25:B1]**.** *AJNR Am J Neuroradiol* 2004;25:214–21
23. Provencher SW. **Estimation of metabolite concentrations from localized in vivo proton NMR spectra.** *Magn Reson Med* 1993;30:672–79
24. Kleihues P, Soylemezoglu F, Schauble B, et al. **Histopathology, classification, and grading of gliomas.** *Glia* 1995;15:211–21
25. Louis DN, Holland EC, Cairncross JG. **Glioma classification: a molecular reappraisal.** *Am J Pathol* 2001;159:779–86
26. Warmuth C, Gunther M, Zimmer C. **Quantification of blood flow in brain tumors: comparison of arterial spin labeling and dynamic susceptibility-weighted contrast-enhanced MR imaging.** *Radiology* 2003;228:523–32
27. Runge VM, Clanton JA, Price AC, et al. **The use of Gd DTPA as a perfusion agent and marker of blood-brain barrier disruption.** *Magn Reson Imaging* 1985;3:43–55
28. Cha S, Knopp EA, Johnson G, et al. **Intracranial mass lesions: dynamic contrast-enhanced susceptibility-weighted echo-planar perfusion MR imaging.** *Radiology* 2002;223:11–29
29. Engelhard HH, Stelea A, Cochran EJ. **Oligodendroglioma: pathology and molecular biology.** *Surg Neurol* 2002;58:111–17
30. von Deimling A, Louis DN, von Ammon K, et al. **Evidence for a tumor suppressor gene on chromosome 19q associated with human astrocytomas, oligodendrogliomas, and mixed gliomas.** *Cancer Res* 1992;52:4277–79
31. Kraus JA, Koopmann J, Kaskel P, et al. **Shared allelic losses on chromosomes 1p and 19q suggest a common origin of oligodendroglioma and oligoastrocytoma.** *J Neuropathol Exp Neurol* 1995;54:91–95
32. Rosenberg JE, Lisle DK, Burwick JA, et al. **Refined deletion mapping of the chromosome 19q glioma tumor suppressor gene to the D19S412-STD interval.** *Oncogene* 1996;13:2483–85
33. Reifenberger J, Reifenberger G, Liu L, et al. **Molecular genetic analysis of oligodendroglial tumors shows preferential allelic deletions on 19q and 1p.** *Am J Pathol* 1994;145:1175–90
34. Daumas-Duport C, Tucker ML, Kolles H, et al. **Oligodendrogliomas. Part II: A new grading system based on morphological and imaging criteria.** *J Neurooncol* 1997;34:61–78
35. Poptani H, Gupta RK, Roy R, et al. **Characterization of intracranial mass lesions with in vivo proton MR spectroscopy.** *AJNR Am J Neuroradiol* 1995;16:1593–603
36. Hall WA, Martin A, Liu H, et al. **Improving diagnostic yield in brain biopsy: coupling spectroscopic targeting with real-time needle placement.** *J Magn Reson Imaging* 2001;13:12–15
37. Michaelis T, Merboldt KD, Bruhn H, et al. **Absolute concentrations of metabolites in the adult human brain in vivo: quantification of localized proton MR spectra.** *Radiology* 1993;187:219–27
38. Miller BL. **A review of chemical issues in 1H NMR spectroscopy: N-acetyl-L-aspartate, creatine and choline.** *NMR Biomed* 1991;4:47–52
39. Nishizuka Y. **Membrane phospholipid degradation and protein kinase C for cell signalling.** *Neurosci Res* 1992;15:3–5
40. Podo F. **Tumour phospholipid metabolism.** *NMR Biomed* 1999;12:413–39
41. Henry RG, Vigneron DB, Fischbein NJ, et al. **Comparison of relative cerebral blood volume and proton spectroscopy in patients with treated gliomas.** *AJNR Am J Neuroradiol* 2000;21:357–66
42. Folkman J. **Tumor angiogenesis.** *Adv Cancer Res* 1974;19:331–58
43. Zagzag D, Zhong H, Scalzitti JM, et al. **Expression of hypoxia-inducible factor 1alpha in brain tumors: association with angiogenesis, invasion, and progression.** *Cancer* 2000;88:2606–18
44. Kuesel AC, Sutherland GR, Halliday W, et al. **1H MRS of high grade astrocytomas: mobile lipid accumulation in necrotic tissue.** *NMR Biomed* 1994;7:149–55
45. Majós C, Alonso J, Aguilera C, et al. **Adult primitive neuroectodermal tumor: proton MR spectroscopic findings with possible application for differential diagnosis.** *Radiology* 2002;225:556–66
46. Likavcanová K, Dobrota D, Liptaj T, et al. **In vitro study of astrocytic tumour metabolism by proton magnetic resonance spectroscopy.** *Gen Physiol Biophys* 2005;24:327–35
47. Lehnhardt FG, Bock C, Rohn G, et al. **Metabolic differences between primary and recurrent human brain tumors: a 1H NMR spectroscopic investigation.** *NMR Biomed* 2005;18:371–82
48. Bouzier AK, Quesson B, Valeins H, et al. [**1-(13)C]glucose metabolism in the tumoral and nontumoral cerebral tissue of a glioma-bearing rat.** *J Neurochem* 1999;72:2445–55
49. Medina MA, Marquez J, Nunez de Castro I. **Interchange of amino acids between tumor and host.** *Biochem Med Metab Biol* 1992;48:1–7
50. Souba WW. **Glutamine and cancer.** *Ann Surg* 1993;218:715–28
51. Ye ZC, Sontheimer H. **Glioma cells release excitotoxic concentrations of glutamate.** *Cancer Res* 1999;59:4383–91
52. Majós C, Alonso J, Aguilera C, et al. **Proton magnetic resonance spectroscopy ((1)H MRS) of human brain tumours: assessment of differences between tumour types and its applicability in brain tumour categorization.** *Eur Radiol* 2003;13:582–91
53. Hagberg G, Burlina AP, Mader I, et al. **In vivo proton MR spectroscopy of human gliomas: definition of metabolic coordinates for multi-dimensional classification.** *Magn Reson Med* 1995;34:242–52
54. Majós C, Julia-Sape M, Alonso J, et al. **Brain tumor classification by proton MR spectroscopy: comparison of diagnostic accuracy at short and long TE.** *AJNR Am J Neuroradiol* 2004;25:1696–704
55. Stadlbauer A, Gruber S, Nimsky C, et al. **Preoperative grading of gliomas by using metabolite quantification with high-spatial-resolution proton MR spectroscopic imaging.** *Radiology* 2006;238:958–69